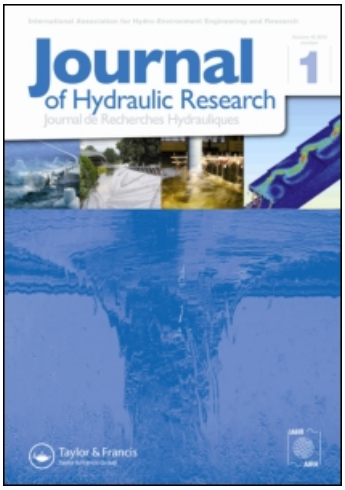

Journal of Hydraulic Research
Publication details, including instructions for authors and subscription information:
http://www.informaworld.com/smpp/title~content=t916282780

Predicting near-field dam-break flow and impact force using a 3D model

Chen Yang[a]; Binliang Lin[b]; Chunbo Jiang[a]; Ying Liu[a]
[a] State Key Laboratory of Hydroscience and Engineering, Tsinghua University, Beijing, People's Republic of China [b] School of Engineering, Cardiff University, Cardiff, UK

Online publication date: 13 December 2010

To cite this Article Yang, Chen , Lin, Binliang , Jiang, Chunbo and Liu, Ying(2010) 'Predicting near-field dam-break flow and impact force using a 3D model', Journal of Hydraulic Research, 48: 6, 784 — 792
To link to this Article: DOI: 10.1080/00221686.2010.531099
URL: http://dx.doi.org/10.1080/00221686.2010.531099

Journal of Hydraulic Research Vol. 48, No. 6 (2010), pp. 784–792
doi:10.1080/00221686.2010.531099

Research paper

Predicting near-field dam-break flow and impact force using a 3D model

CHEN YANG, PhD Student, *State Key Laboratory of Hydroscience and Engineering, Tsinghua University, Beijing 100084, People's Republic of China.*
Email: yangchen07@mails.tsinghua.edu.cn

BINLIANG LIN (IAHR Member), Professor, *School of Engineering, Cardiff University, Cardiff CF24 3AA, UK.*
Email: linbl@cardiff.ac.uk (author for correspondence)

CHUNBO JIANG, Professor, *State Key Laboratory of Hydroscience and Engineering, Tsinghua University, Beijing 100084, People's Republic of China.*
Email: jcb@mail.tsinghua.edu.cn

YING LIU, Graduate Student, *State Key Laboratory of Hydroscience and Engineering, Tsinghua University, Beijing 100084, People's Republic of China.*
Email: liuying08@mails.tsinghua.edu.cn

ABSTRACT
A three-dimensional (3D) numerical model based on the unsteady Reynolds equations was used to simulate near-field dam-break flows and estimate the impact force on obstacles. The model employs a projection method to solve the governing equations and the method of volume of fluid (VOF) to capture the water surface movement. The model is first applied to simulate two physical model experiments of dam-break flows. Model-predicted pressure, water depth and velocity distributions are compared with laboratory measurements. For the second case, the 3D-VOF model predictions are also compared with predictions made by a two-dimensional model. The 3D-VOF model is then used to calculate the impact force of dam-break flow on a steady obstacle. A physical model experiment is set up to assist the numerical model study. The model-predicted impact force on the obstacle and the critical condition for it to move are compared with the measurements from the experiment.

Keywords: Dam-break flow, flume experiment, impact force, VOF method, 3D model

1 Introduction

A dam-break flow corresponds to an uncontrolled release of water due to a dam, a dyke or other types of hydraulic structure failures. The resulting rapid water-level increase creates serious floods, with sharp gradient wave fronts and significant impact forces on structures or obstacles. From the hydrodynamic point of view, dam-break flows normally involve shockwaves and sub-critical, supercritical and trans-critical flows. Both analytical and numerical models were used to predict dam-break flows in idealized conditions (Lauber and Hager 1998), with numerical models being also capable of predicting more complex dam-break flows.

Two-dimensional (2D) depth-integrated hydrodynamic models, originally developed to simulate unsteady shallow-water flows, were used to compute flood propagation along rivers and floodplains. These models have been gradually adapted to sharp gradient surface flows, including dam-break flood waves. A growing number of such models are currently being used to simulate natural flows such as flash floods (Hogg and Pritchard 2004), floods with sediment transport (Pritchard 2005), snow avalanches (Bartelt *et al.* 1999), debris flows (Huang and García 1997, Iverson 1997) and lava flows (Griffiths 2000). In recent years, many numerical methods have been developed to simulate dam-break flows, including the characteristics method (Katopodes and Strelkoff 1978, 1979), finite-difference method (Aureli *et al.* 2000, Macchione and Morelli 2003, Liang *et al.* 2007a, 2007b, 2007c), discrete finite-element method (Cockburn *et al.* 2000, Dawson and Martinez-Canales 2000) and finite-volume method (Zhou *et al.* 1996, Wang and Liu 2001, Medina *et al.* 2008). Hervouet and Petitjean

Revision received 8 October 2010/Open for discussion until 30 June 2011.

ISSN 0022-1686 print/ISSN 1814-2079 online
http://www.informaworld.com

(1999) presented 2D model simulations of Malpasset dam-break flows using the software package TELEMAC-2D. The study concludes that the 2D model is capable of simulating flood-waves over large floodplains of some tens of kilometres in length.

Although depth-averaged shallow water flow models can be used to simulate dam-break flows, they have limitations. This is due to the fact that a number of assumptions are used in deriving the shallow water equations (SWE). Among them, the most important are: long-wave approximation, i.e. no significant curvature of free surface, hydrostatic pressure distribution and mild velocity profile. For flows involving a considerable variation in flow depth in the vertical direction, such as near-field dam-break flows, the above assumptions may not always hold. Due to the rapid propagation speed, dam-break flows induce significant impact force on structures or obstacles. Thus, a reliable estimation of the impact forces is important for flood risk assessment. However, due to the hydrostatic pressure assumption, the capability of 2D shallow water models is limited in dealing with (i) rapid surface-level changes in their vicinity and (ii) dynamic pressure distribution at the water and structures or obstacles interfaces. These limitations may affect the 2D model accuracy in computing the impact forces.

For depth-averaged 2D models, it is relatively straightforward to locate the free surface, as the water depth is one of the unknowns in the 2D hydrodynamic equations. The location of the free surface is known once the solution of the hydrodynamic equations is found. However, the water depth is not explicitly included in the 3D hydrodynamic equations, thus extra effort is needed to locate the free surface. Recently, efforts focused on numerically predicting the formation and propagation of shock waves by explicitly capturing the free surface. According to the way in which the surface is reconstructed in the model, free-surface-capturing methods can be generally classified as: (1) free-surface-tracking approach or (2) discharge-tracking approach. Approach (1) involves coordinate transformation, e.g. numerical conformal mapping, but it is rarely used in simulating flows around obstacles, because of the difficulty in dealing with the multiple-value problem when water flows over and under an obstacle. Approach (2) is more widely used, which includes the marker and cell method (Harlow *et al.* 1965), volume of fluid (VOF) method (Hirt and Nichols 1981) and level-set method (Osher and Sethian 1998). Approach (2) was used in simulating surface wave propagation and wave–structure interaction, because it is capable of dealing with the problems of free surface rolling over and breaking. Time-averaged turbulent models and large-eddy simulation models were used in these models to simulate the interaction between waves and structures (Armenio 1998). Tao and Xie (1999) and Yuan and Tao (2000) employed the level-set method to simulate 2D vertical dam-break flows. A three-dimensional (3D) numerical model based on solving Reynolds equations and the VOF method was developed by Yang *et al.* (2006) to simulate the interaction between short period waves and small-diameter cylinders.

The aim of this study is to assess the performance of the 3D-VOF model by Yang *et al.* (2006) for simulating near-field dam-break flows and the associated impact force on steady obstacles. In Section 2, details of the governing equations, boundary conditions and the solution method used are given. Model applications to two laboratory experiments are presented in Section 3. One is a near-field dam-break flow experiment conducted by the present authors, whereas the other is a dam-break flow experiment conducted in a channel with a sudden enlargement by Soares Frazão *et al.* (2003). In Section 4, the model is used to determine the impact of dam-break flow induced force on steady obstacles. Details of a laboratory experiment and the numerical model simulation undertaken to determine the impact force on an obstacle are given. Comparisons are made between model predictions and experimental results. Section 5 summarizes the main findings of this study.

2 Numerical model

2.1 *Governing equations*

As described above, 3D models are required to simulate rapidly-varying near-field flows and the forces impacted on structures or obstacles in a dam-break flow situation. Furthermore, dam-break waves may reflect as they hit an obstacle, and the water surface changes sharply. The flow regime is generally turbulent; thus, a high Reynolds number turbulence model is used herein. The numerical model is based on the 3D Reynolds equations. The turbulence model used is the two equation k-ε model. For 3D flows, for which the length scale cannot be prescribed empirically in an easy way, two equation models are the simplest turbulence models that promise success (ASCE Task Committee on Turbulence Models in Hydraulic Computations 1988).

In Cartesian coordinates, the governing equations for the fluid flow are expressed as:

Continuity equation

$$\frac{\partial u_i}{\partial x_i} = 0 \tag{1}$$

Momentum equations

$$\frac{\partial u_i}{\partial t} + u_j \frac{\partial u_i}{\partial x_j} = -\frac{1}{\rho}\frac{\partial p}{\partial x_i} + g_i + \frac{\partial \tau_{ij}}{\partial x_j} \tag{2}$$

k-ε equations

$$\frac{\partial k}{\partial t} + u_j \frac{\partial k}{\partial x_j} = \frac{\partial}{\partial x_j}\left[\left(\frac{\upsilon_t}{\sigma_k} + \upsilon\right)\frac{\partial k}{\partial x_j}\right] + G - \varepsilon \tag{3}$$

$$\frac{\partial \varepsilon}{\partial t} + u_j \frac{\partial \varepsilon}{\partial x_j} = \frac{\partial}{\partial x_j}\left[\left(\frac{\upsilon_t}{\sigma_\varepsilon} + \upsilon\right)\frac{\partial \varepsilon}{\partial x_j}\right] + C_{1\varepsilon}\frac{\varepsilon}{k}G - C_{2\varepsilon}\frac{\varepsilon^2}{k} \tag{4}$$

in which

$$\tau_{ij} = 2(\upsilon + \upsilon_t)\sigma_{ij} - \frac{2}{3}k\delta_{ij}$$

$$G = 2\upsilon_t \sigma_{ij} \frac{\partial u_i}{\partial x_j}$$

$$\sigma_{ij} = \frac{1}{2}\left(\frac{\partial u_i}{\partial x_j} + \frac{\partial u_j}{\partial x_i}\right)$$

$$\upsilon_t = C_d \frac{k^2}{\varepsilon}$$

where k = turbulent kinetic energy, ε = turbulent energy dissipation rate, G = rate of production of turbulence kinetic energy, $i = 1, 2, 3$, $j = 1, 2, 3$, δ_{ij} = Kronecker delta function, υ = kinematic viscosity, υ_t = eddy viscosity, u_i = velocity component in the ith direction, p = pressure, ρ = fluid density, g_i = component of gravity acceleration in the ith direction, $g_1 = g_2 = 0$, $g_3 = -g$. The coefficients in Eqs. (3) and (4) are chosen based on the "standard k-ε model" by Launder and Spalding (1974) as $C_d = 0.09$, $C_{1g} = 1.44$, $C_{2g} = 1.92$, $\sigma_k = 1.00$, $\sigma_\varepsilon = 1.30$. The standard k-ε model is one of the most widely tested and successfully applied turbulence models. Its predictive capabilities for many near-field situations are well established (ASCE Task Committee on Turbulence Models in Hydraulic Computations 1988).

2.2 *Boundary conditions*

For the dam-break problems concerned in this study, the following boundary conditions are used:

1) At the water surface, the following kinetic and dynamic boundary conditions are satisfied

$$\frac{\partial \eta}{\partial t} + u_j \frac{\partial \eta}{\partial x_j} = 0 \tag{5}$$

$$\begin{aligned} p - \upsilon_t\left(\frac{\partial u_i}{\partial x_j} + \frac{\partial u_j}{\partial x_i}\right)n_i n_j &= \tau_n \\ \upsilon_t\left(\frac{\partial u_i}{\partial x_j} + \frac{\partial u_j}{\partial x_i}\right)n_i t_j &= \tau_t \end{aligned} \tag{6}$$

   in which η is the free surface elevation, n_i, $n_j = (n_1, n_2, n_3)$ and $t_j = (t_1, t_2, t_3)$ are normal and tangential unit vector of the water surface, respectively, τ_n and τ_t = normal and tangential stress acting on the water surface, respectively.
2) The wall function (Launder and Spalding 1974) is adopted within the near-wall region, where the velocity is described by the logarithmic law.
3) At the upstream boundary, the flow velocity is set to zero.
4) At the outflow boundary, the flow is assumed to be fully developed, with a zero normal gradient specified for all flow variables.

2.3 *Free-surface-tracking method*

The VOF method is used to track the free surface. A function $f = f(x_1, x_2, x_3, t)$ is defined at each point within the model domain. If a point is occupied by water, $f = 1$, and $f = 0$ otherwise. Within each cell, a function is defined to represent the volume fraction of fluid, namely

$$F(x_1, x_2, x_3, t) = \frac{1}{\Delta V}\iiint_{\Delta V} f(\varsigma, \eta, \zeta, t)\mathrm{d}\varsigma\mathrm{d}\eta\mathrm{d}\zeta \tag{7}$$

where ΔV is the cell volume. The free surface lies in a cell if the F value at this cell is between 0 and 1. The transport equation of F is

$$\frac{\partial F}{\partial t} + \frac{\partial u_i F}{\partial x_i} = 0 \tag{8}$$

By solving Eq. (8), the location of the free surface is determined. However, F cannot be solved by any regular discrete difference scheme because it is a step function. Therefore, it is solved in two steps, first by an advection step and then a reconstruction step. At the advection step, new volume fraction values are first calculated using the F values and interface configuration obtained from the previous step. The new interface is then reconstructed from the new volume fraction field. In this study, the SOLA-VOF method proposed by Hirt and Nichols (1981) is used. The interface within each cell is thereby represented as either a vertical or a horizontal surface, the direction of which depends only on the spatial gradient of volume fraction F.

2.4 *Solution method*

The computation domain is discretized into cuboid cells. Within a cell, all scalar variables (p, k, ε, υ_t, and the VOF function F) are located in the cell centre and the vector quantities are located on the middle points of the side faces . The Reynolds equations are solved by a two-step projection method. In the first step, the ith direction momentum equation is used to find an intermediate velocity,

$$\frac{\hat{u}_i^{n+1} - u_i^n}{\Delta t} = -u_j^n \frac{\partial u_i^n}{\partial x_j} + g_i + \frac{\partial \tau_{ij}^n}{\partial x_j} \tag{9}$$

in which the superscript n indicates the time level and Δt is the time step. At this stage, the continuity equation is not satisfied yet.

The second step is to project the intermediate velocity field onto a divergence-free plane to obtain the final velocity

$$\frac{u_i^{n+1} - \hat{u}_i^{n+1}}{\Delta t} = -\frac{1}{\rho^n}\frac{\partial p^{n+1}}{\partial x_i} \tag{10}$$

$$\frac{\partial u_i^{n+1}}{\partial x_i} = 0 \tag{11}$$

It can be demonstrated that by combining Eqs. (9) and (10) the Reynolds equations are approximately satisfied. Taking the

divergence of Eq. (10) and applying Eq. (11) to the resulting equation yield the Poisson pressure equation

$$\frac{\partial}{\partial x_i}\left(\frac{1}{\rho^n}+\frac{\partial p^{n+1}}{\partial x_i}\right)=\frac{1}{\Delta t}\frac{\partial \hat{u}_i^{n+1}}{\partial x_i} \tag{12}$$

The k, ε equations (3) and (4) are discretized as

$$\frac{k_{ij}^{n+1}-k_{ij}^{n}}{\Delta t}=-k_x-k_y+k_{vis}+\frac{1}{2}(G_{ij}^{n+1}+G_{ij}^{n}-\varepsilon_{ij}^{n+1}-\varepsilon_{ij}^{n}) \tag{13}$$

$$\frac{\varepsilon_{ij}^{n+1}-\varepsilon_{ij}^{n}}{\Delta t}=-\varepsilon_x-\varepsilon_y+\varepsilon_{vis}+C_{1\varepsilon}\frac{\varepsilon_{ij}^{n}}{k_{ij}^{n}}G_{ij}^{n+1}-C_{2\varepsilon}\frac{\varepsilon_{ij}^{n}}{k_{ij}^{n}}\varepsilon_{ij}^{n+1} \tag{14}$$

In Eq. (13), k_x and k_y = advection terms of the turbulent kinetic energy k in the x- and y-directions, respectively, and k_{vis} = diffusion terms of k. In Eq. (14), ε_x and ε_y = advection terms of the turbulent dissipation rate ε in the x- and y-directions, respectively, and ε_{dis} = diffusion terms of ε.

3 Dam-break simulations

The 3D-VOF model was applied to two test cases to simulate near-field dam-break flows. In case 1, the model was applied to a small-scale dam-break problem, for which a flume experiment was first conducted to provide data. In case 2, the model was applied to a laboratory experiment conducted by Soares Frazão *et al.* (2003). The 3D model predictions were also compared with predictions obtained from a depth-integrated 2D model.

3.1 *Case 1: dam-break flow in a rectangular channel*

This experiment was carried out in a 28 m long, 1.6 m wide and 1 m deep flume (Fig. 1). Its side walls were made of glass and the bed was of concrete. A 1.0 m high dam was built 10 m from the upstream flume end to separate the reservoir from the floodplain. The dam had a 0.2 m wide gap. A flood gate, made of wood and rubber, was used to control the upstream water level. Initially, the reservoir water level was set to 0.4 m and the water level in the floodplain downstream of the dam was set to 0.12 m. The aim of this experiment was to observe the free surface and pressure and velocity fields. Twenty-one pressure-sensing probes were embedded in the floodplain bed to record the instant dynamic pressure distributions. The pressure probes can sense and record the instant pressure with a maximum frequency of 50 Hz. The surface velocity field was captured by a velocity dynamic measurement system (VDMS) based on the particle image velocimetry (PIV) technology. A commercial software package was used to transform images to velocity fields. The software was first set up jointly with the VDMS and calibrated before the experiment. Three cameras were used to record the velocity field. White 0.5 cm diameter plastic wafers were used as tracers for velocity measurement.

The flood gate was removed manually at the beginning of each experiment. The average time for the gate to be lifted out of the water was found to be about 0.24 s. According to Lauber and Hager (1998), this time period can be considered as instantaneous. After the gate was removed, the dam-break wave spread quickly along the channel. The wave front reached the flume end and was reflected into the domain of interest within $t \cong 20$ s. Thus, only the experimental data collected in the first 20 s were used.

The numerical model deployed a regular rectangular grid of 80,000 ($160 \times 50 \times 10$) points. The time step was set to 0.01 s and the total computational time for each run was about 10 min using a 2.4 GHz PC. Model predictions indicated that after the dam was suddenly removed, the water level just behind the wave front increased rapidly, while the water level within the reservoir gradually decreased. The water level behind the wave front reduced gradually with time, in agreement with pressure measurements as discussed below.

Figure 2 shows the measured dynamic pressure distributions and the corresponding numerical model predictions at two typical gauging points, i.e. points 11 and 18 (Fig. 1a). At point 11, the flood wave front arrived at about 1.0 s after the gate was removed. Initially, the pressure increased slowly. From $t = 1.4$ s, the pressure started to increase rapidly, until the pressure head had reached 0.21 m at $t = 2.3$ s. The pressure then decreased, yet with some oscillations, until the pressure head was reduced to about 0.154 m at $t = 20$ s. At point 18, the pattern of pressure change was similar to that at point 11, but the pressure wave arrived about 0.5 s later. The model-predicted dynamic pressure distributions agree generally well with the test measurements. At the rapid pressure increase phase, the model-predicted slope increase was slightly steeper than that measured. This is likely to be due to the fact that the numerical model assumed an instant flood gate release while in the experiment it took about 0.24 s to release the gate. During the pressure-decreasing phase, the model was able to predict the average pressure values, but less well the oscillations recorded by the pressure probes.

The model-predicted velocity fields were then compared with these obtained by the digital PIV. Due to the large quantity of data involved and memory limitation, the velocity field was captured only once in every 10 s. Thus, for each experiment, two frames of velocity field were captured at (i) $t = 2.5$ s and (ii) $t = 12.5$ s. Because of the high flow speed just downstream of the gate and the steep slope of the flood wave front, the tracer particles in some regions were not captured by cameras.

Figure 3 compares model-predicted and measured velocity fields at the water surface, at $t = 2.5$ s. Comparing with the pressure predictions, the model-predicted surface velocity

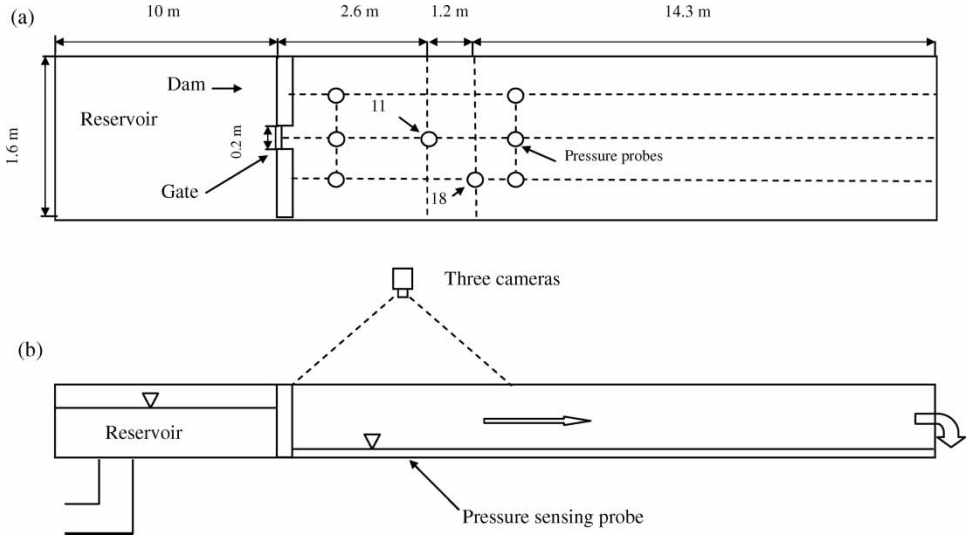

Figure 1 Experimental set-up and selected gauging points: (a) top view and (b) side view

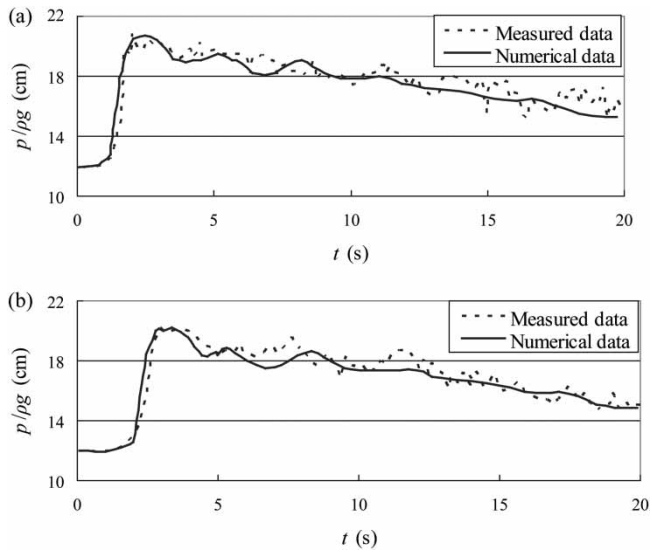

Figure 2 Comparisons between model-predicted pressure distributions and experimental measurements at gauging points (a) 11 and (b) 18

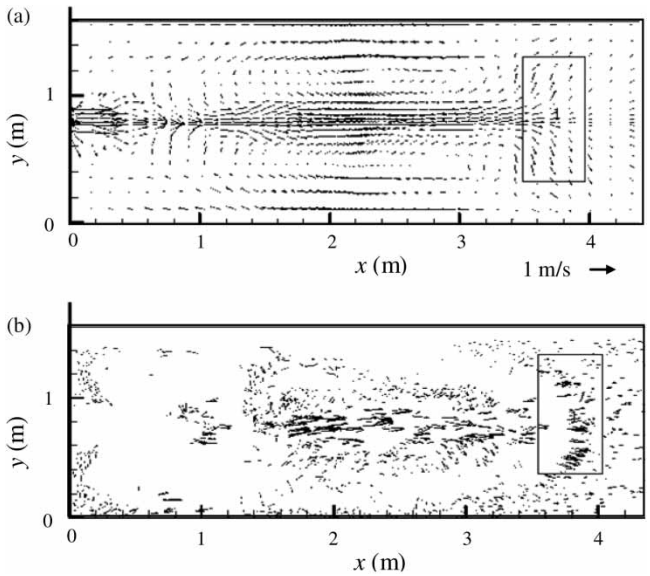

Figure 3 (a) Predicted and (b) measured velocity field at $t = 2.5$°s

fields agrees less well with the experimental results. This is thought to be partly due to the fact that the experimental results were snapshots at the water surface, while the numerical model predictions were based on velocities over the volume of the top layer cells. Nevertheless, the key features were captured by the numerical model. At $t = 2.5$ s, the camera-captured position of the wave front (rectangular boxes on the right side of Fig. 3) and the large flow velocities at the central channel portion were correctly predicted by the numerical model. It was also found that at $t = 12.5$ s, the model-predicted vortex regimes largely agree with the test image. At the initial stage of model simulation, small magnitude oscillations are observed at the wave front, due to the steep gradient of water level caused by the sudden gate removal. The oscillations disappeared as the wave front moved forward.

From laboratory and numerical model results, it was observed that the dam-break flows were turbulent near the flood gate. Thus, a turbulence model is necessary for simulating near-field dam-break flows. However, the predicted velocity distributions are smoother than the observations. This is thought to be partly due to the homogeneous eddy viscosity employed in the standard k-ε model.

3.2 *Case 2: dam-break flows in channel with sudden enlargement*

Soares Frazão *et al.* (2003) conducted a series of laboratory experiments to investigate dam-break flows. They also undertook numerical model simulations using a 2D model called Roe2D-2oT. In the present study, the 3D-VOF numerical

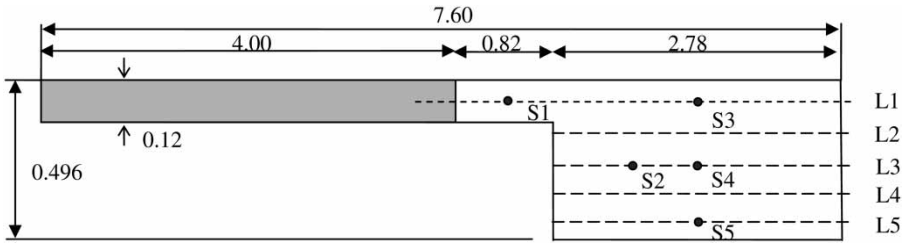

Figure 4 Experimental set-up and position of gauging points in metre (Soares Frazao *et al.* 2003)

model was used to predict the flow field for one of their experiments. The 3D model predictions were compared with the experimental data and the 2D numerical model results published by Soares Frazão *et al.* (2003).

The flume was 7.6 m long with an enlargement 4.82 m from the upstream end and a gate located at 4.0 m from the upstream end (Fig. 4). Five water-level gauges were used to record water levels at selected points, S1–S5, and a digital imaging method was used to obtain the surface-velocity field. The dam-break flow test simulated herein had an initial water depth of 0.20 m in the reservoir and an initially dry bed in the floodplain. The Manning coefficient was 0.015 $\mathrm{sm}^{-1/3}$ (Soares Frazão *et al.* 2003).

In Fig. 5, numerical model-predicted water levels at gauging points S2 and S4 are compared with the measurements, resulting from both the 3D-VOF model and Roe2D-2oT model by Soares Frazão *et al.* (2003). The results from the Roe2D-2oT model agree with the experimental results well for most of the simulation time, but a delay is observed in the arrival time of the hydraulic jump. The 3D-VOF model predicted slightly better the sharp increase in water level at the wave front and the timing of the hydraulic jump, due to the improved accuracy in capturing the free surface by using the VOF method.

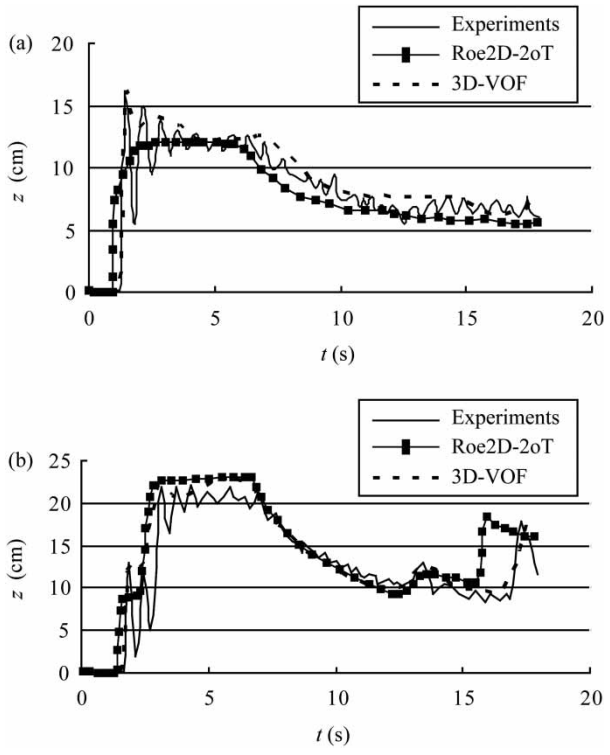

Figure 5 Comparison between experimental measurements and different numerical results at (a) gauge S2 and (b) gauge S4

A comparison was also made between the surface velocity field predicted by the 3D model and the surface-velocity field captured from the experiment by Soares Frazão *et al.* (2003), with the numerical model-predicted flow pattern agreeing quite well with the observations. Although depth-averaged 2D models can also be used to predict such dam-break flows, they are unable to predict the vertical distribution of the velocity field. For some near-field dam-break flow problems, e.g. sediment transport-induced bed erosion, a good knowledge of the vertical velocity distribution is beneficial.

It should be pointed out that near the wave front the vertical pressure distribution is non-hydrostatic due to the rapid change of water depth. Figure 6 shows the predicted vertical pressure distribution at gauging point S4 at $t = 1.75$ s. Note that the vertical pressure distribution is nonlinear. Therefore, it can be concluded that, although 2D models based on the hydrostatic pressure assumption could be used to simulate the propagation of dam-break flows, a 3D model capable of predicting non-hydrostatic pressure distributions should be used for predicting vertical pressure distributions in near-field dam-break flows. This is especially true if the pressure distribution is to be employed to calculate the impact force on structures or obstacles.

4 Impact force calculation

In a dam-break flow situation, structures or obstacles located near the dam may suffer huge impact force because of the significant

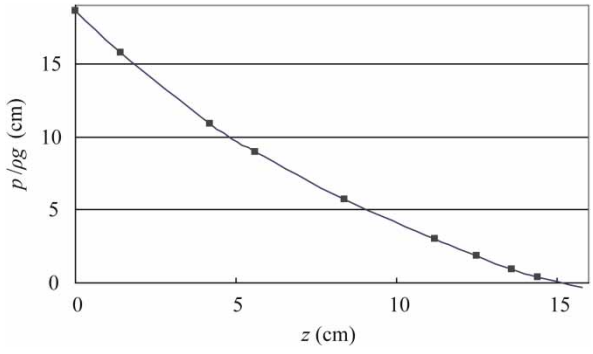

Figure 6 Predicted pressure distribution at gauging point S4 at 1.75 s

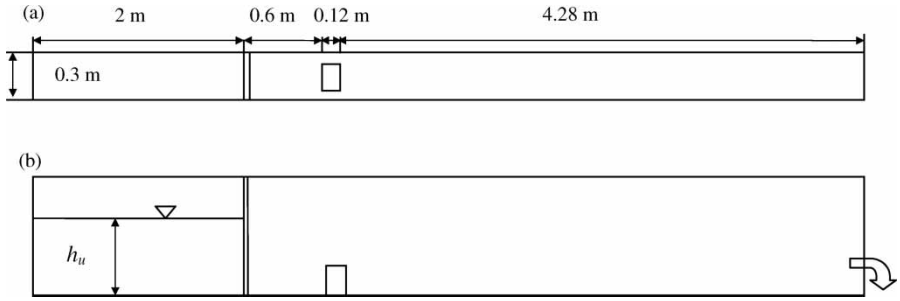

Figure 7 Experimental set-up, (a) top view, (b) side view

energy carried by the flow. Traditional 2D numerical models based on the SWE are generally unable to calculate such an impact. Thus, the 3D-VOF numerical model was used herein to simulate the impact forces. The stress on the obstacle surface cell was determined using the pressure and velocity fields obtained by the 3D numerical model according to

$$p_{ij} = \begin{cases} -p + 2\upsilon_t\left(\dfrac{\partial u_i}{\partial x_j} - \dfrac{1}{3}\dfrac{\partial u_j}{\partial x_j}\right) & i = j \\ \upsilon_t\left(\dfrac{\partial u_j}{\partial x_i} + \dfrac{\partial u_i}{\partial x_j}\right) & i \neq j \end{cases} \tag{15}$$

The total impact force in the x_i-direction F_i was obtained by summing the forces on the entire interface cells (including both normal and shear forces) between the obstacle and water in the x_i-direction.

To estimate the performance of the present numerical model in calculating dam-break flow-induced impact forces, a laboratory experiment was conducted. It was conducted in a flume of 7 m × 0.3 m × 0.5 m (Fig. 7). The upstream flume portion was first closed to form a reservoir. A brick measured at 0.22 m × 0.12 m × 0.07 m of weight 2.73 kg was initially placed 0.6 m downstream. The resistance force of the channel bed to the brick in still water was measured in advance using a spring scale. The resulting relationship between the resistance force and the still water depth is shown in Fig. 8. Due to the buoyancy of the brick, the force required to move the brick depresses as the water level increases. As the water level reaches the brick height of 0.07 m, the force required to move the brick becomes constant.

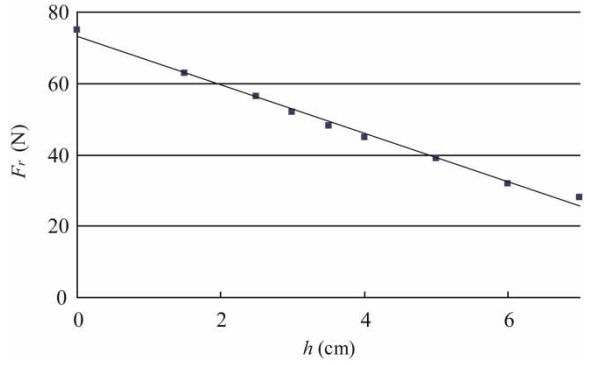

Figure 8 Resistance forces of brick F_r in water of various depths

The friction coefficient λ between the channel bed and the brick was calculated based on Fig. 8 using

$$F_r = \lambda(Wt - F_f) \tag{16}$$

where Wt = weight of brick, Fr = resistance of brick (i.e. obtained from reading the spring scale) as the brick starts to move, F_f = buoyancy force, which was calculated as

$$F_f = \rho_w g s_b h \tag{17}$$

where ρ_w = density of water, s_b = basal brick area, and h = water depth around brick. From Fig. 8, $\lambda = 2.813$. Experiments were then conducted with various initial reservoir water depths h_u. At each critical depth, a flood test was carried out by suddenly opening the gate and recording the initial brick movement. It was found that the critical reservoir water depth causing the brick to move was about 0.123 m. Several tests were then conducted to confirm this depth. The 3D-VOF model was then used to simulate the experiment. The impact force in the main flow direction F_i was obtained based on Eq. (15). The resistance force F_r was computed using Eqs. (16) and (17).

A series of numerical model simulations were then undertaken, with the initial reservoir water depth being gradually increased. If $F_i > F_r$, then the brick was assumed to be able to move, and vice versa. The critical reservoir water depth h_u for the brick to move was found to be 0.135 m, which is 9.76% larger than 0.123 m. The difference is mainly because (1) a mean water depth was used to calculate the brick buoyancy, (2) the brick roughness was not taken into account for calculating the shear force at the interface between the brick and water and (3) small measurement errors.

Figure 9 shows the model-predicted impact force and the bed resistance force for $h_u = 0.135$ m. Note that the resistance force decreases as the water level around the brick increases and there is a rapid increase in the impact force as the flood wave front passes the brick. The impact force catches up with the resistance force at $t = 0.48$ s. At this moment, the brick was about to move. The model predicted initial reservoir level required for the obstacle to move agreed relatively well with the experiments,

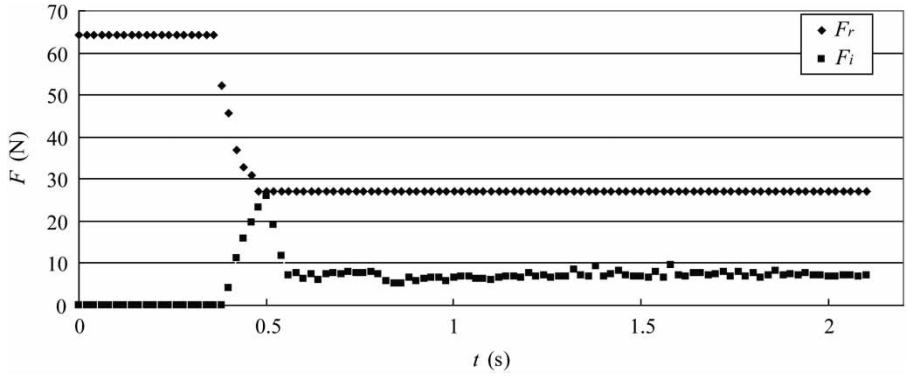

Figure 9 Predicted resistance and impact forces for reservoir level of 0.135 m

indicating that the present 3D-VOF model can be used to estimate dam-break flow induced impact.

5 Conclusions

A 3D numerical model based on the unsteady Reynolds equations was used to simulate near-field dam-break flows and associate impact force on steady obstacles. The model was applied to three tests. The first was to simulate a dam-break flow experiment conducted by the authors. Model-predicted pressure distributions at the floodplain bed agreed with the experimental measurements generally well. However, the predictions of the surface velocity distributions agreed less well. Nevertheless, similar flow patterns could still be observed between model-predicted and measured velocity fields.

In the second test, the 3D-VOF model was used to simulate a dam-break flow experiment for a non-symmetrical floodplain. In addition to experimental measurements, the 3D model predictions were also compared with predictions by a 2D model. The 3D-VOF model performed slightly better than the 2D model in predicting the sharp increase in water level at the wave front and the timing of the hydraulic jump. This is thought to be due to the improved accuracy in capturing the free surface by using the VOF method. The model results also indicate that the pressure distribution is non-hydrostatic in the near field.

In the third test, the model was used to estimate flood flow-induced impact force on hydraulic structures or obstacles. A flume dam-break flow experiment was conducted to estimate the impact force exerted on a steady obstacle. The 3D-VOF model was used to predict the impact force on the obstacle and the critical initial reservoir level required for the obstacle to move. The model-predicted condition for the obstacle to move agreed relatively well with experimentation. Note that the results presented herein have uncertainties and limitations. In test 1, the surface-velocity fields captured by the PIV system involved relatively high level of uncertainties, and in test 3, the dam-break-induced impact force was estimated indirectly by initial reservoir levels. Improvement will be made in future studies.

Acknowledgement

This research was supported by the National Key Basic Research Project of China (973 Project, 2006CB403304), Tsinghua University Initiative Scientific Research Program (2009THZ07060) and the State Key Laboratory of Hydroscience and Engineering, Tsinghua University (2008-ZY-5, 2009-TC-2).

Notation

f = 1 if a point is occupied by water, otherwise $f = 0$
F_f = buoyancy of brick
F_i = impact force in the x_i-direction
F_r = resistance
G = production rate of turbulence kinetic energy
g_i = component of gravitational acceleration in the ith direction
$\bar{h}$ = mean water depth around the obstacle
h_b = water depth behind the obstacle
h_f = water depth in front of the obstacle
h_u = initial water depth within the reservoir
k = turbulent kinetic energy
n_j = (n_1, n_2, n_3) = vertical unit vector of water surface
p = pressure
s_b = basal area of the obstacle
t_j = (t_1, t_2, t_3) = tangential unit vector of water surface
u_i = velocity component in the ith direction
$\hat{u}_i^{n+1}$ = intermediate velocity
Wt = weight of the obstacle
x = distance in the x-direction
y = distance in the y-direction
z = distance in the z-direction
η = distance from free surface to datum
ρ = fluid density
υ = kinetic viscosity
ε = turbulent energy dissipation rate
δ_{ij} = Kronecker delta function
υ_t = eddy viscosity
τ_n = vertical stress acting on water surface

τ_t = tangential stress acting on water surface
ΔV = cell volume
λ = resistance coefficient
ρ_w = density of water

References

Armenio, V. (1998). Dynamic loads on submerged bodies in a viscous numerical wave tank at small KC numbers. *Ocean Eng*. 25(10), 881–905.

ASCE Task Committee on Turbulence Models in Hydraulic Computations (1988). Turbulence modeling of surface water flow and transport: Part 2. *J. Hydraulic Eng*. 114(9), 992–1014.

Aureli, F., Mignosa, P., Tomirotti, M. (2000). Numerical simulation and experimental verification of dam-break flows with shocks. *J. Hydraulic Res*. 38(3), 197–206.

Bartelt, P., Salm, B., Gruber, U. (1999). Calculating dense-snow avalanche runoff using a Voellmy-fluid model with active passive longitudinal straining. *J. Glaciology* 45(150), 242–254.

Cockburn, B., Karniadakis, G.E., Shu, C.W. (2000). *Discontinuous Galerkin methods:* Theory, computation and application. Brown University, Providence RI.

Dawson, C.N., Martinez-Canales, M.L. (2000). A characteristic-Galerkin approximation to a system of shallow water equations. *Numerische Mathematik* 86(2), 239–256.

Griffiths, R. (2000). The dynamics of lava flows. *Annul Review of Fluid Mech*. 32, 477–518.

Harlow, F., Shannon, J., Welch, J. (1965). THE MAC METHOD: A computing technique for solving viscous, incompressible, transient fluid-flow problems involving free surfaces. *Technical Report* LA-3425. Los Alamos Scientific Laboratory, Los Alamos NM.

Hervouet, J.M., Petitjean, A. (1999). Malpasset dam-break revisited with two-dimensional computations. *J. Hydraulic Res*. 37(6), 377–388.

Hirt, C.W., Nichols, B.D. (1981). Volume of Fluid (VOF) Method for the dynamics of free boundaries. *J. Computat. Phys*. 39(1), 201–225.

Hogg, A.J., Pritchard, D. (2004). The effects of hydraulic resistance on dam-break and other shallow inertial flows. *J. Fluid Mech*. 501, 179–212.

Huang, X., García, M. (1997). A perturbation solution for Bingham plastic mudflows. *J. Hydraulic Eng*. 123(11), 986–994.

Iverson, R. (1997). The physics of debris flows. *Review of Geophysics* 35(3), 245–296.

Katopodes, N., Strelkoff, T. (1978). Computing two-dimensional dam-break flood waves. *J. Eng. Mech. Div*. ASCE 104(EM9), 1269–1288.

Katopodes, N., Strelkoff, T. (1979). Two-dimensional shallow water-wave models. *J. Eng. Mech. Div*. ASCE 105(EM2), 317–334.

Lauber, G., Hager, W.H. (1998). Experiments to dam break wave: Horizontal channel. *J. Hydraulic Res*. 36(3), 291–307.

Launder, B.E., Spalding, D.B. (1974). The numerical computation of turbulent flows. *Comp. Meth. in Appl. Mech. and Eng*. 3(2), 269–289.

Liang, D.F., Lin, B.L., Falconer, R.A. (2007a). A boundary-fitted numerical model for flood routing with shock-capturing capability. *J. Hydrology* 332(3-4), 477–486.

Liang, D.F., Falconer, R.A., Lin, B.L. (2007b). Coupling surface and subsurface flows in a depth averaged flood wave model. *J. Hydrology* 337(1-2), 147–158.

Liang, D.F., Lin, B.L., Falconer, R.A. (2007c). Simulation of rapidly varying flow using an efficient TVD-MacCormack scheme. *Intl. J. Numer. Meth. in Fluids* 53(5), 811–826.

Macchione, F., Morelli, M.A. (2003). Practical aspects in comparing shock-capturing schemes for dam-break problems. *J. Hydraulic Eng*. 129(3), 187–195.

Medina, V., Hürlimann, M., Bateman, A. (2008). Application of FLATModel, a 2D finite volume code to debris flows in the north eastern part of the Liberian Peninsula. *Landslides* 5, 127–142.

Osher, S., Sethian, J.A. (1998). Fronts propagating with curvature-dependent speed: Algorithms based on Hamilton-Jacobi formulations. *J. of Comput. Physics* 79(1), 12–49.

Pritchard, D. (2005). On fine sediment transport by a flood surge. *J. Fluid Mech*. 543, 239–248.

Soares Frazão, S., Lories, D., Taminiau, S., Zech, Y. (2003). Dam-break flow in a channel with a sudden enlargement. Proc. 30th *IAHR Congress* Thessaloniki, Greece C(II), 221–228.

Tao, J.H., Xie, W.S. (1999). Simulation of propagation dam-break waves using Level Set method. *J. Hydraulic Eng*. 10, 17–22 [in Chinese].

Wang, J.W., Liu, R.X. (2001). The composite finite volume method on unstructured triangular meshes for 2D shallow water equations. *Intl. J. Numer. Methods in Fluids* 37(8), 933–949.

Yang, C., Liu, C.G., Tao, J.H. (2006). Simulation of save forces on arrays of small-diameter cylinders by using 3D unsteady Reynolds equations. *J. Hydrodynamics* 21(6), 781–788 [in Chinese].

Yuan, D.K., Tao, J.H. (2000). Simulation of the flow with free surface by Level Set method. *Chinese Journal of Theoretical and Applied Mechanics* 32(3), 262–271 [in Chinese].

Zhou, D.H., Shen, H.W., Lai, J.S., Tabios, III. G.Q. (1996). Approximate Riemann solvers in FVM for 2D hydraulic shock wave modelling. *J. Hydraulic Eng*. 122(12), 692–702.